THE JOURNAL OF PHYSICAL CHEMISTRY Letters

Letter

pubs.acs.org/JPCL

Optical Trap-Mediated High-Sensitivity Nanohole Array Biosensors with Random Nanospikes

Takayasu Yoshikawa,[†] Mamoru Tamura,*[,†] Shiho Tokonami,[‡] and Takuya Iida*[,†]

[†]Department of Physical Science, Graduate School of Science and [‡]Department of Applied Chemistry, Graduate School of Engineering, Osaka Prefecture University, 1-1 Gakuen-cho, Naka-ku, Sakai, Osaka 599-8531, Japan

ABSTRACT: We clarify an unconventional principle of the light-driven operation of a biosensor for enhanced sensitivity with the help of random nanospikes added to the surface of a nanohole array. Such a system is capable of optically guiding viruses and trapping them in the vicinity of a highly sensitive site by an anomalous light-induced force arising from random-nanospike-modulated extraordinary optical transmission and the plasmonic mirror image in a virus as a dielectric submicron object. In particular, after guiding the viruses near the apex of nanospikes, there are conditions where the spectral peak shift of extraordinary optical transmission can be greatly increased and reach several hundred nanometers in comparison with that of a conventional nanohole array without random nanospikes. These results will allow for the development of a simple, rapid, and highly sensitive virus detection method based on optical trapping with the help of random-nanospike-modulated extraordinary optical transmission, facilitating convenient medical diagnosis and food inspection.

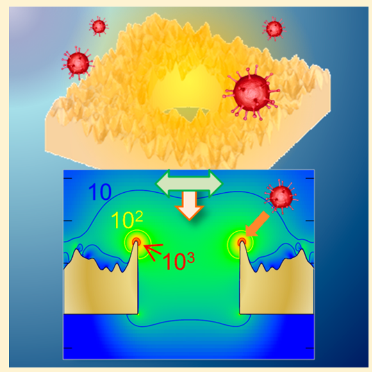

A lot of research on biosensors for virus detection has been recently reported in fields such as clinical examination, environmental measurement, food inspection, and biosecurity. Conventional techniques to identify pathogenic viruses have already been put to practical use on both laboratorial and widespread commercial levels.[1,2] That is the case, for example, for the enzyme-linked immunosorbent assay (ELISA) method with high specificity for proteins, identifying pathogenic viruses by amplification of DNA in the sample solution via a polymerase chain reaction. However, these methods are still hampered by many problems such as the complexity of the detection process, the cost of the fluorescent materials used for detection, difficulties in the specific detection of unknown or mutated viruses, and the detection methods depending on the environment.[3] To improve such optical sensing technologies, a sample optical response coupled with surface plasmon resonance (SPR) in metallic nanostructures has been actively studied; sensitive and label-free detection methods have thus been developed, based on the spectral changes in SPR.[4] In particular, a SPR-based technique named extraordinary optical transmission (EOT) is attracting much attention because of its potential application in sensors.[5] In EOT, a metallic thin film with a periodic array of nanoscale holes, that is, a nanohole array (NHA), is used, which exhibits strong optical transmission properties at a particular wavelength. This phenomenon can be considered to result from the coupled mode of the localized surface plasmon and propagating surface plasmon, where the resonant wavelength of EOT depends on the refractive index of the surrounding medium. Therefore, the spectral peak shift in the EOT facilitates the specific detection of target viruses when combined with selective capture of the target viruses by antigen−antibody reactions on an antibody-modified metallic film with NHA.[6,7] The NHA-based sensor can be realized with simpler configurations than conventional SPR-based sensors. For example, the Kretschmann configuration in a traditional SPR sensor requires a prism with oblique light incidence to detect targets,[8] whereas the NHA-based sensor requires only normal incidence.

It is well-known that the properties of localized SPR depend strongly on the shape of the used metallic nanostructures; a sharp pointed metallic structure, for example, can confine and enhance the electric field of incident light in the vicinity of the apex. In addition, when a dielectric object approaches the apex, a well-known spectral shift based on the localized SPR mirror image in the dielectric occurs; this phenomenon can be employed in high-density optical storage[9] and is also very promising in NHA-based sensors. On the other hand, the metallic nanoparticles can be densely and uniformly fixed on the surface of micron objects,[10,11] and their strong optical response has been employed in the detection of nanoscale biological targets such as DNA[12] and proteins.[13] The sensitivity of these sensors will be improved by strong localized light fields around metallic nanostructures with a small curvature radius.[14] In particular, a large spectral shift would be expected by the adhesion of small biological targets to a sharp plasmonic nanostructure like a spike structure.[15,16] There is also the further possibility of increasing sensor sensitivity by optically guiding the viruses and trapping them in the vicinity of a highly sensitive site like the apex region of a nanoscale spike, based on the optical trapping by light-induced force (LIF).[17−21] A NHA-based sensor improved by dielectrophoresis has been reported,[22] which requires additional experimental equipment

Received: October 2, 2016
Accepted: December 12, 2016

DOI: 10.1021/acs.jpclett.6b02262
J. Phys. Chem. Lett. 2017, 8, 370−374

such as electrodes and oscillators in addition to the optical system. However, optical trapping-mediated detection enables us to remotely control the target and requires only the optical system without electrodes.

Here, using these mechanisms to explore an unconventional scheme for the sensitive detection of viruses, we investigate the optical response of the coupled system of a NHA with random nanospikes (RNSs) and a virus assumed as a dielectric submicron object in conjunction with the optical guiding of a target toward the observation region. We compare the spectral modulations of EOT in the proposed NHA in the presence of RNSs with those of the conventional NHA without RNSs, based on the finite difference time domain (FDTD) method,[23] and the LIF acting on the target objects is evaluated using the Maxwell stress tensor (MST) method.[24]

To understand the difference in optical response of the conventional NHA sensor (without RNSs, Figure 1a) and the proposed NHA sensor (with RNSs, Figure 1b), the transmittance T of both sensors was evaluated under irradiation with an x-polarized plane wave propagating in the $-z$ direction. The sensor areas shown in these figures correspond to the unit cell of the FDTD simulations, where the following parameters were used in the NHA model: a nanohole diameter of 240 nm, a film thickness of 120 nm, and a spatial period of 600 nm for the nanoholes. In Figure 1b, an undulation of RNSs in the NHA surface is given as follows: the average z-position of RNS was adjusted to the surface shown in Figure 1a, and the average height was 18 nm, with an average period of 30 nm. These values were carefully selected via preliminary calculations to increase the sensitivity to as high as possible. A periodic boundary condition was imposed on the x–y plane, whereas a perfect matched layer was imposed on the z-boundary. The dielectric function of gold was obtained by fitting the experimental data of Johnson and Christy.[25] The surrounding medium was assumed to be water (refractive index n = 1.33). The edge lengths of the FDTD cubic mesh used for calculations were 1 nm for gold and 1/34 of the shortest wavelength in the calculated spectral range for all other regions. The second vertical axis in Figure 1c shows the transmittance T normalized by T_g (the ratio of hole area to irradiation area, i.e., the geometric transmittance defined from the viewpoint of ray optics considering the film as a perfect reflector). Therefore, a normalized transmittance larger than unity implies that the transmittance does not result from ray propagation in the hole (light cannot propagate in a hole smaller than the half-wavelength, in the first place) but results instead from SPR excitation; thus EOT can be obtained. Figure 1c shows that the peak wavelength of EOT is shifted from peak ⟨A⟩ 910 nm to ⟨B⟩ 1030 nm by RNSs addition. The x–z distributions of the squared amplitude of normalized electric field on a cross section passing through a hole at each EOT peak wavelength are shown in Figure 1d,e. Considering the strongly localized electric field near the RNSs observable in Figure 1e, we can expect the target viruses will be optically guided—and trapped—by the LIF in the vicinity of the RNSs.

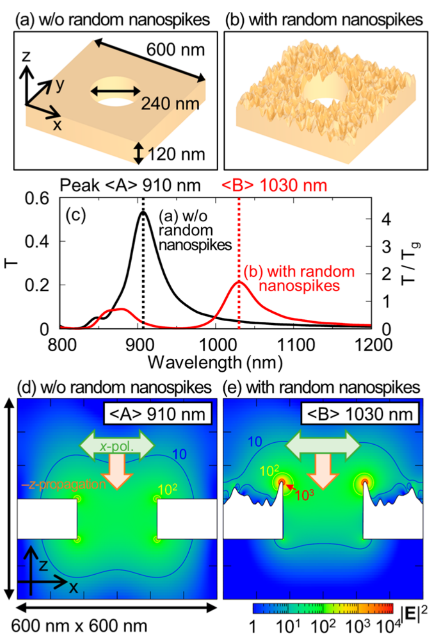

Figure 1. Models of the conventional and proposed NHA sensors and their fundamental optical responses. (a) Unit cell of the conventional model (without spikes). (b) Unit cell of the proposed model with RNSs. (c) Transmittance spectra T of both models, with n = 1.33. (d,e) x–z distributions of the squared amplitude of electric field on cross sections passing through the hole centers of models (a) and (b), respectively, at the peak wavelength of each EOT: ⟨A⟩ 910 nm and ⟨B⟩ 1030 nm.

The spectral changes resulting from virus adhesion were also evaluated. These changes are shown in Figure 2, where the virus is represented by a dielectric sphere with a diameter of 300 nm and a refractive index of 1.58 (similar to the one of a protein); the surrounding medium was changed to air (n = 1) because it was assumed that after virus adhesion in water the virus detection step (based on the spectral change) is performed in dry conditions to increase the refractive index contrast. Three different z-positions of the virus were assumed, to consider the virus supported by the spikes or hole edge, as shown in the insets of Figure 2a–c. However, because the z-position of the virus greatly affects the extent of peak shift, the same positions were assumed for other spike situations. In this regard, the z-position (iii) in Figure 2a,b seems to be an unnatural situation that a virus overlaps spikes. However, because a virus consists of organic soft materials such as proteins, it can be easily deformed by nanospikes, as reported in recent papers using a sharp probe tip[26–28] similar to a nanospike; thus, such overlapping situations are worth considering. In these situations, the dielectric function of the metal overrode the dielectric constant of the virus in the overlapped regions. Figure 2a shows peak shifts of 101 and 233 nm for virus attachment at (i) and (iii), whereas Figure 2c shows 38 and 120 nm for (i) and (iii). This indicates the possibility of large enhancement of the peak shift by the RNSs in the range from 101 to 233 nm and confirms that RNSs improve detection sensitivity. In addition, to clarify the contribution of the nanospikes to the enhancement in the peak shift, ideal nanospikes (INSs) were considered, where "ideal" implies that the location of the nanospikes is ideal to reproduce the spectrum behavior in the presence of RNSs. Figure 2b indicates that INSs can also enhance the peak shift in the range from 154 to 234 nm for (ii) and (iii). Interestingly, the spectrum behavior of Figure 2b is very similar to that of Figure 2a, and thus, it can be considered that the RNSs near the hole edge are an especially sensitive region and contribute to the enhancement in peak shift. As a result, in comparison with the peak shift of 120 nm in Figure 2c, there is a possibility that the amount of peak shift is largely increased in the range from

DOI: 10.1021/acs.jpclett.6b02262
J. Phys. Chem. Lett. 2017, 8, 370–374

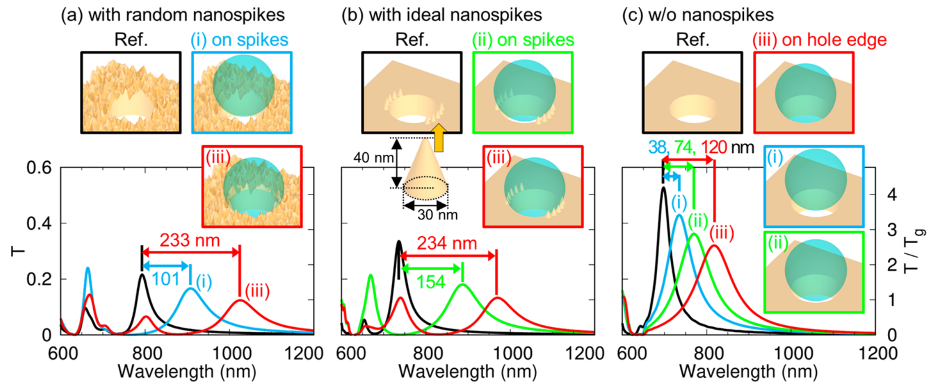

Figure 2. Spectra of NHA transmittance before (black) and after (colored) spherical virus attachment. (a) With RNSs. (b) With INSs. (c) Without nanospikes. The three different *z*-positions of virus (i), (ii), and (iii) were determined to place the virus on each metal structures of (a), (b), and (c), respectively. The second vertical axis represents the normalized transmittance.

101 to 233 nm or from 154 to 234 nm by using RNSs or INSs, as shown in Figure 2a,b. These peak shifts are attributed to the interaction between a real image of localized surface plasmon in RNSs or INSs and its mirror image in a spherical virus, and the high dielectric constant of the virus close to a nanospike greatly increases the strength of the mirror image effect.[9,29]

The case for the adhesion of multiple viruses was also considered. To compare the optical responses of NHAs with and without RNSs independently of any particular adhesion location, a film-shaped virus aggregate was assumed in Figure 3a,b (as shown in the insets of these figures); in this case, the

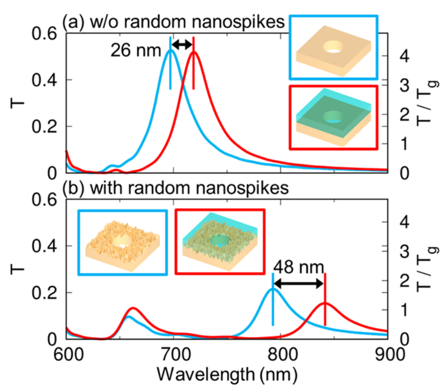

Figure 3. Spectra of NHA transmittance for a film-shaped virus aggregates attachment. (a) Without nanospikes. (b) With RNSs. The plots are similar to those in Figure 2. The film thickness is 100 nm except for the rough surface region in (b), where the bottom of the film-shaped virus aggregate is fitted to the roughness.

refractive index of virus was changed to 1.1, under the assumption that viruses adhere sparsely and randomly and that their refractive index can be averaged in a manner similar to the effective medium approximation. Further, in this case, the peak shift was increased from 26 to 48 nm in the presence of RNSs. These results indicate the possibility of great improvements in the virus detection sensitivity of NHAs when the virus is located in the vicinity of a sharp nanoscale structure.

To clarify the possibility of optically guiding the target viruses, the LIFs acting on the viruses in water (n = 1.33) were evaluated using the MST method, as per the following equation[18,24]

$$\langle \mathbf{F} \rangle = \langle \int_S \mathrm{d}S\ \mathbf{T}\cdot\mathbf{n} \rangle \tag{1}$$

where $\mathbf{T} = \mathbf{EE} + \mathbf{HH} - (1/2)(|\mathbf{E}|^2 + |\mathbf{H}|^2)\mathbf{I}$, $\mathbf{E}$ and $\mathbf{H}$ are the response electric and magnetic fields, S is the surface area of a virtual cube surrounding each dielectric sphere (the model for a virus), and $\mathbf{n}$ is the unit normal vector of surface S. Figure 4a

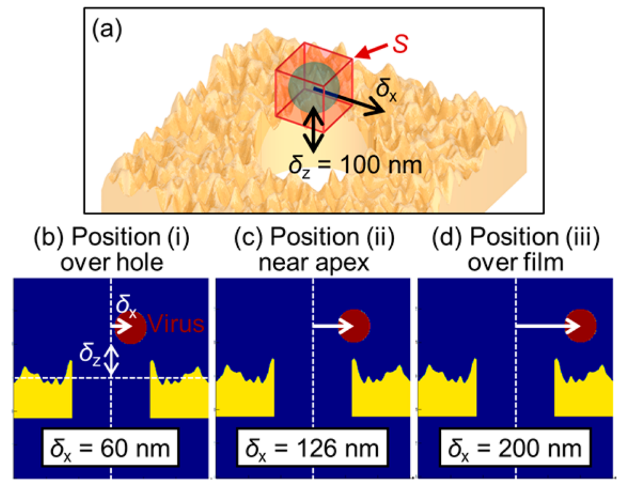

Figure 4. (a) Virus model used to calculate the LIF with the MST. (b−d) Three different virus positions used to calculate the LIF: (i) over the hole, (ii) near the apex, and (iii) over the film. (δ_x is the horizontal distance between the virus and the nanohole center.).

shows the overall calculation model, with the virus being represented by a dielectric sphere with a diameter of 100 nm and a refractive index of 1.58, located over the film at a distance of δ_z = 100 nm from the average RNS height, where the size of a virus sphere was smaller to investigate the contribution of a single apex. A laser intensity of 12.7 kW/cm^2 was used in the simulation, which corresponds to a laser intensity having 0.1 mW of power and a spot diameter of 1 μm. Three different x-positions (i)−(iii) were considered for the virus, as shown in Figure 4b−d. The calculated results of the x- and z-components of the LIFs acting on the virus for each of the three considered locations are shown in Figure 5, together with the transmittance spectra. The dissipative force in the light propagation direction ($-z$ direction) resonantly pushes the virus toward the surface of the NHA, and the horizontal gradient force (along the x direction) attracts the virus to the apex of the RNS even though the sphere intrinsically has no resonance in this wavelength region. For the EOT wavelength 1031 nm corresponding to the peak ⟨B⟩ in Figure 1c, the LIF x-component is positive for

DOI: 10.1021/acs.jpclett.6b02262
J. Phys. Chem. Lett. 2017, 8, 370−374

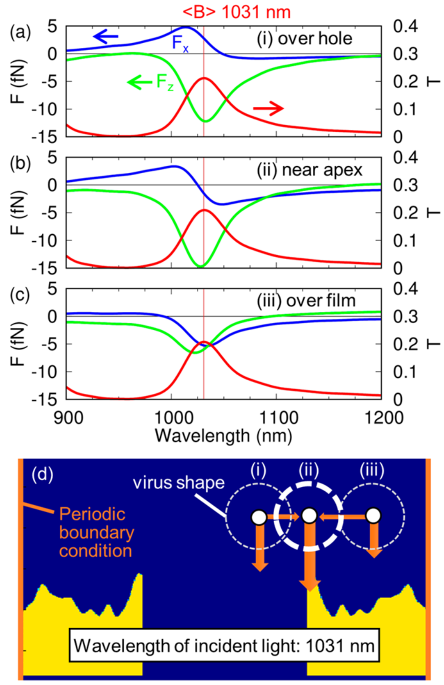

Figure 5. Results of the MST calculation. (a−c) LIF *x*- and *z*-components and transmittance spectra for three different virus positions. (d) Schematic image of the LIF *x*- and *z*-components for 1031 nm light, in accordance with (a−c).

position (i) and negative for position (iii), whereas it is almost zero for position (ii), as shown in Figure 5a−c. On the other hand, the *z*-component of the LIF is negative in all cases (the same as the light propagation direction) and is especially stronger for positions (i) and (ii). This result indicates the possibility to optically guide floating viruses in water toward the RNS apex under the laser irradiation of the EOT peak wavelength (as illustrated in Figure 5d). The fact that the EOT peak shift caused by the addition of RNS (shown in Figure 1c) can be controlled by the RNS height and period allows the adjustment of the EOT peak wavelength to a desired value. Therefore, choosing, for example, 1064 nm, which is a typical wavelength of the infrared laser for optical tweezers, the NHA sensor can be easily combined with a simple system of optical manipulation. Such a peak shift mechanism can be explained by an analytical calculation with a discrete dipole approximation[9,29] that such an enhancement of the LIF results from the mirror image of the coupled mode of the localized SPR and propagating SPR as the origin of EOT in a virus dielectric sphere, when the virus gets close to the RNSs. Further, it has been confirmed that each component of the LIF by a RNS-added NHA can be twice as large as that by the flat surface NHA without RNSs at the same *z*-position. These results indicate that the synergetic effect of the mirror image and EOT can be used for highly efficient optical guidance to the sensitive detection site.

In conclusion, we have clarified the possibility of a highly sensitive random-nanospike-added nanohole array virus sensor with the help of optically guided trapping viruses in water using light-induced force under extraordinary optical transmission modulated by the mirror image effect. The spectral peak shift caused by virus adhesion to nanospikes near a nanohole can be significantly increased from several tens of nanometers to more than a hundred nanometer after drying in comparison with the conventional system without random nanospikes. The mechanism can facilitate the development of a low-cost, simple, rapid, and high-throughput virus detection method even in the case of low virus concentrations since the self-assembling method can be used for the production of random nanospikes on the surface of the nanohole array. It is noteworthy to point out that the optically guided trapping effect is achievable even with a defocused, low-power vertical incident laser by using a simple optical system. The presented results and the increased comprehension of the phenomena involved will lead to the development of localized light-guided nanohole array sensors based on the trapping effect of light-induced force and the enhanced peak shift obtained by the synergetic effect of mirror image and extraordinary optical transmission. The discussed principles will certainly foster the appearance of future alternative methods for practical field diagnostics and thus prevent the diffusion of various infectious diseases.

■ AUTHOR INFORMATION

Corresponding Authors

*E-mail: t-iida@p.s.osakafu-u.ac.jp (T.I.).

*E-mail: m-tamura@p.s.osakafu-u.ac.jp (M.T.)

ORCID

Takuya Iida: 0000-0003-1313-7025

Notes

The authors declare no competing financial interest.

■ ACKNOWLEDGMENTS

The authors would like to thank Dr. N. D. Vy, Mr. K. Nishida, and Prof. K. Imura for their helpful discussions from theoretical and experimental viewpoints. We also thank Prof. H. Ishihara for his encouragement and support. This work was supported by a Grant-in-Aid for Scientific Research (B) (No. 26286029 and No. 15H03010), a Grants-in-Aid for Exploratory Research (No. 24654091, No.15K14697, and No. 16K14340), a Grant-in-Aid for JSPS Fellows (No. 14J08760), Scientific Research on Innovative Areas "Nano-Material Optical-Manipulation" (No. 16H06507) from JSPS KAKENHI, the Canon Foundation, the Key Project Grant Program of Osaka Prefecture University, and the Cooperative Research Program of "Network Joint Research Center for Materials and Devices".

■ REFERENCES

(1) Byrne, B.; Stack, E.; Gilmartin, N.; O'Kennedy, R. Antibody-based Sensors: Principles, Problems and Potential for Detection of Pathogens and Associated Toxins. *Sensors* **2009**, *9*, 4407−4445.

(2) Emmerson, G. D.; Sparrow, I. J. G.; Bhatta, D.; SohnaSohna, J. E. Novel Optical Sensors for Detection of Toxins, Viruses, and Bacteria. *Proc. SPIE* **2008**, *7116*, 711603.

(3) Kaushik, A.; Tiwari, S.; Dev Jayant, R.; Marty, A.; Nair, M. Towards Detection and Diagnosis of Ebola Virus Disease at Point-of-care. *Biosens. Bioelectron.* **2016**, *75*, 254−272.

(4) Fan, X.; White, I. M.; Shopova, S. I.; Zhu, H.; Suter, J. D.; Sun, Y. Sensitive Optical Biosensors for Unlabeled Targets: A Review. *Anal. Chim. Acta* **2008**, *620*, 8−26.

(5) Ebbesen, T. W.; Lezec, H. J.; Ghaemi, H. F.; Thio, T.; Wolff, P. A. Extraordinary Optical Transmission Through Sub-wavelength Hole Arrays. *Nature* **1998**, *391*, 667−669.

(6) Yanik, A. A.; Huang, M.; Kamohara, O.; Artar, A.; Geisbert, T. W.; Connor, J. H.; Altug, H. An Optofluidic Nanoplasmonic Biosensor for Direct Detection of Live Viruses from Biological Media. *Nano Lett.* **2010**, *10*, 4962−4969.

(7) Escobedo, C. On-chip Nanohole Array Based Sensing: A Review. *Lab Chip* **2013**, *13*, 2445−2463.

DOI: 10.1021/acs.jpclett.6b02262
J. Phys. Chem. Lett. 2017, 8, 370−374

(8) Brolo, A. G. Plasmonics for Future Biosensors. *Nat. Photonics* **2012**, *6*, 709−713.

(9) Iida, T.; Nakamura, A.; Hidaka, S.; Tamura, M.; Shiono, T.; Furumiya, S. Enhanced Modulation of Scattered Light from Phase-change Nanoparticles by Tailored Plasmonic Mirror Image. *Appl. Phys. Lett.* **2013**, *103*, 041108.

(10) Tokonami, S.; Yamamoto, Y.; Mizutani, Y.; Ota, I.; Shiigi, H.; Nagaoka, T. Green Electroless Plating Method Using Gold Nanoparticles for Conducting Microbeads: Application to Anisotropic Conductive Films. *J. Electrochem. Soc.* **2009**, *156*, D558−D563.

(11) Shiigi, H.; Fukuda, M.; Tono, T.; Takada, K.; Okada, T.; Dung, L. Q.; Hatsuoka, Y.; Kinoshita, T.; Takai, M.; Tokonami, S.; Nakao, H.; Nishino, T.; Yamamoto, Y.; Nagaoka, T. Construction of Nanoantennas on the Bacterial Outer Membrane. *Chem. Commun.* **2014**, *50*, 6252−6255.

(12) Tokonami, S.; Nishida, K.; Hidaka, S.; Yamamoto, Y.; Nakao, H.; Iida, T. DNA-mediated Anomalous Optical Coupling of Heterogeneous Metallic Nanostructures. *J. Phys. Chem. C* **2014**, *118*, 7235−7241.

(13) Nishimura, Y.; Nishida, K.; Yamamoto, Y.; Ito, S.; Tokonami, S.; Iida, T. Control of Submillimeter Phase Transition by Collective Photothermal Effect. *J. Phys. Chem. C* **2014**, *118*, 18799−18804.

(14) Kawata, S. *Near-Field Optics and Surface Plasmon Polaritons*; Springer: Berlin, Germany, 2001.

(15) Sabri, Y. M.; Kandjani, A. E.; Ippolito, S. J.; Bhargava, S. K. Ordered Monolayer Gold Nano-urchin Structures and Their Size Induced Control for High Gas Sensing Performance. *Sci. Rep.* **2016**, *6*, 24625.

(16) Novikov, S. M.; Sánchez-Iglesias, A.; Schmidt, M. K.; Chuvilin, A.; Aizpurua, J.; Grzelczak, M.; Liz-Marzán, L. M. Gold Spiky Nanodumbbells: Anisotropy in Gold Nanostars. *Part. Part. Syst. Charact.* **2014**, *31*, 77−80.

(17) Ashkin, A.; Schütze, K.; Dziedzic, J. M.; Euteneuer, U.; Schliwa, M. Force Generation of Organelle Transport Measured in Vivo by an Infrared Laser Trap. *Nature* **1990**, *348*, 346−348.

(18) Iida, T.; Ishihara, H. Theory of Resonant Radiation Force Exerted on Nanostructures by Optical Excitation of Their Quantum States: From Microscopic to Macroscopic Descriptions. *Phys. Rev. B: Condens. Matter Mater. Phys.* **2008**, *77*, 245319/1−245319/16.

(19) Iida, T. Control of Plasmonic Superradiance in Metallic Nanoparticle Assembly by Light-induced Force and Fluctuations. *J. Phys. Chem. Lett.* **2012**, *3*, 332−336.

(20) Tamura, M.; Iida, T. Fluctuation-mediated Optical Screening of Nanoparticles. *Nano Lett.* **2012**, *12*, 5337−5341.

(21) Iida, T.; Ito, S.; Tokonami, S.; Kojima, C. Nano-optomechanics by Tailored Light Fields under Fluctuations. In *Progress in Nanophotonics 3*; Ohtsu, M., Yatsui, T., Eds.; Springer: Berlin, Germany, 2015.

(22) Barik, A.; Otto, L. M.; Yoo, D.; Jose, J.; Johnson, T. W.; Oh, S.-H. Dielectrophoresis-enhanced Plasmonic Sensing with Gold Nanohole Arrays. *Nano Lett.* **2014**, *14*, 2006−2012.

(23) Yee, K. S. Numerical Solution of Initial Boundary Value Problems Involving Maxwell's Equations in Isotropic Media. *IEEE Trans. Antennas Propag.* **1966**, *14*, 302−307.

(24) Iida, T.; Ishihara, H. Optically Induced Force Between Nanoparticles Irradiated by Electronic Resonant Light. *J. Lumin.* **2005**, *112*, 151−155.

(25) Johnson, P. B.; Christy, R. W. Optical Constants of the Noble Metals. *Phys. Rev. B* **1972**, *6*, 4370−4379.

(26) Schaap, I. A.; Eghiaian, F.; des Georges, A.; Veigel, C. Effect of envelope proteins on the mechanical properties of influenza virus. *J. Biol. Chem.* **2012**, *287*, 41078−41088.

(27) Li, S.; Sieben, C.; Ludwig, K.; Höfer; Chris, T.; Chiantia, S.; Herrmann, A.; Eghiaian, F.; Schaap; Iwan, A. T. pH-Controlled Two-Step Uncoating of Influenza Virus. *Biophys. J.* **2014**, *106*, 1447−1456.

(28) Batishchev, O. V.; Shilova, L. A.; Kachala, M. V.; Tashkin, V. Y.; Sokolov, V. S.; Fedorova, N. V.; Baratova, L. A.; Knyazev, D. G.; Zimmerberg, J.; Chizmadzhev, Y. A. pH-Dependent Formation and Disintegration of the Influenza A Virus Protein Scaffold To Provide Tension for Membrane Fusion. *J. Virol.* **2016**, *90*, 575−585.

(29) Kojima, C.; Watanabe, Y.; Hattori, H.; Iida, T. Design of Photosensitive Gold Nanoparticles for Biomedical Applications Based on Self-Consistent Optical Response Theory. *J. Phys. Chem. C* **2011**, *115*, 19091−19095.

DOI: 10.1021/acs.jpclett.6b02262
J. Phys. Chem. Lett. 2017, 8, 370−374